Calculation of internal and scattered fields of axisymmetric nanoparticles at any point in space

K. Holms, B. Hourahine and F. Papoff

Department of Physics, University of Strathclyde, John Anderson Building, 107 Rottenrow, Glasgow, G4 0NG

E-mail: kenny@phys.strath.ac.uk, papoff@phys.strath.ac.uk, benjamin.hourahine@strath.ac.uk

Abstract. We present a method of simultaneously calculating both the internal and external fields of arbitrarily shaped dielectric and metallic axisymmetric nanoparticles. By using a set of distributed spherical vector wave functions that are exact solutions to Maxwell's equations and form a complete, linearly independent set on the particle surface, we approximate the surface Green functions of particles. In this way we can enforce the boundary conditions at the interface and represent the electromagnetic fields at the surface to an arbitrary precision. With the boundary conditions at the particle surface satisfied, the electromagnetic fields are uniquely determined at any point in space, whether internal or external to the particle. Furthermore, the residual field error at the particle surface can be shown to give an upper bound error for the field solutions at any point in space. We show the accuracy of this method with two important areas studied widely in literature, photonic nanojets and the internal field structure of nano-particles.

Keywords: Scattering, surface Green functions, near field.

Submitted to: *J. Opt. A: Pure Appl. Opt.*

1. Introduction

There has been constant interest in the field of nano-optics since the publication of Mie's seminal paper describing scattering from nanoparticles [1]. Recent advances in production techniques have led to the manufacture of nanoparticles with vast ranges of sizes, shapes and materials. This broad range of nanoparticles display a wide variety of interesting optical properties. Metallic nanostructures, for instance, due to their highly tunable particle resonances have near field applications such as surface enhancement of fluorescence and Raman scattering [2]. Another near field effect that has been of significant interest recently is the formation of photonic nanojets [3], which are intense, narrow beams emerging from the shadow side of illuminated dielectric nanoparticles. These jets can appear for a wide range of particle parameters and show great potential applications in sub-wavelength resolution microscopy [4] and super high density optical data storage [5]. Aside from these near field effects, accurately modelling the far field properties of nanoparticles is of great interest in many different fields. In atmospherics, the ability to study how satellite communications are effected by clouds, dust and ice are of importance [6]. Also, the investigation of the optical properties of cosmic dust grains detected in astronomical objects are of importance to astrophysics [7].

Optical properties can be calculated via many different methods but a particular technique may only be suitable for a specific region of space or specific type of particle. The Finite Difference Time Domain technique (FDFT) [8], for instance, is one of the most popular methods of finding the near field properties, but it is computationally demanding, able to find the fields only on on a predefined grid, and must be calculated for each different incident field. The T-matrix or Null Field method with Discrete Sources (NFM-DS) [9] is widely used for calculating the properties of elongated particles. However, this method can only find the fields of interest outside a particle's smallest circumscribing sphere, which severely limits the near field information for elongated particles. Existing surface Green function methods which use localised sources [10],[11] have the advantage of being able to find the fields at any point in space, but are limited to particles of low aspect ratio due to the use of functions defined at the origin of coordinates to enforce the boundary conditions, which produce an ill conditioned set of equations for elongated particles.

In this paper we present a new method of calculating approximate surface Green functions for homogeneous particles via a distributed set of functions and Moore-Penrose pseudo-inverse matrices. In this way, the electromagnetic fields can be determined with high precision at all points in space, even for metallic or for very elongated dielectric particles.

2. Theory

2.1. Maxwell's equations and boundary conditions

We can write Maxwell's equations as

$$\nabla \times \begin{bmatrix} \mathbf{E} \\ \mathbf{H} \end{bmatrix} = ik_t \begin{bmatrix} 0 & \sqrt{\frac{\mu^t}{\epsilon^t}} \\ -\sqrt{\frac{\epsilon^t}{\mu^t}} & 0 \end{bmatrix} \begin{bmatrix} \mathbf{E} \\ \mathbf{H} \end{bmatrix}, \tag{1}$$

with $k_t = \omega\sqrt{\epsilon^t \mu^t}$ and $t = i$ or $t = s$ where i corresponds to an internal field and s is a scattered field.

At the interface between penetrable materials such as dielectrics and metals with finite conductivity, the tangential components of the electromagnetic fields are continuous, i.e. the fields are subject to the boundary conditions:

$$\hat{\mathbf{n}}(p) \times (\mathbf{E^0}(p) + \mathbf{E^s}(p)) = \hat{\mathbf{n}}(p) \times \mathbf{E^i}(p), \tag{2}$$

$$\hat{\mathbf{n}}(p) \times (\mathbf{H^0}(p) + \mathbf{H^s}(p)) = \hat{\mathbf{n}}(p) \times \mathbf{H^i}(p),, \tag{3}$$

where p is a point on the surface and $\hat{\mathbf{n}}(p)$ is the unitary normal to the surface at p.

2.2. Particle geometry and field expansions

A diagramatical representation of a typical elongated axisymmetric nanostructure in shown in Fig. 1, along with the location of distributed Spherical Vector Wave Function (SVWF) sources within the particle. Due to the symmetry of the particle, the

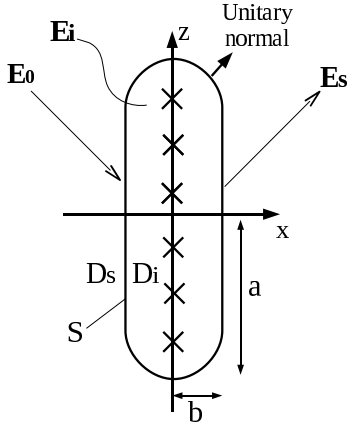

Figure 1. Typical geometry of an axisymmetric particle showing the surface of the scatterer S separating the interior domain D_i from the exterior domain D_s, and the unitary normal $\hat{\mathbf{n}}$ at a point on the surface. The fields of interest, $E_{i,s}$ are the internal and scattered fields and are expanded in terms of the distributed SVWF's with origins marked by crosses. The major and minor axes of the particle are a and b, respectively.

azimuthal modes decouple and the problem can be solved for each mode individually. The distributed SVWF's are the lowest order functions for each azimuthal mode in question, $\mathbf{M}_{l=max(1,|m|),m}$ and $\mathbf{N}_{l=max(1,|m|),m}$: they are complete and linearly independent at the particle surface if it is sufficiently smooth, as well as being exact solutions to Maxwell's equations [12].

Consider the set of vectors in compact notation; $|F^t_\nu >= [M^t_\nu, -i\mathcal{C}^t N^t_\nu]$ for $1 \leq \nu \leq \nu^t_{Max}$ and $|F^t_\nu >= [N^t_\nu, -i\mathcal{C}^t M^t_\nu]$ for $\nu^t_{Max}+1 \leq \nu \leq 2\nu^t_{Max}$ where ν is an index that takes into account the index of the SVWF source point and the azimuthal mode, $2\nu^t_{Max}$ is the total number of functions used in the expansion, and $\mathcal{C}^t = \sqrt{\epsilon^t/\mu^t}$. In terms of this notation, the explicit form of the field expansions in terms of distributed lowest order SVWF's is

$$\mathcal{F}^{\mathbf{t}} = \begin{bmatrix} \mathbf{E}^t \\ \mathbf{H}^t \end{bmatrix} = c^t_\nu |F^t_\nu >, \tag{4}$$

where c^t_ν are the expansion coefficients, and we sum over repeated indices.

2.3. Surface Green Functions

The surface Green function (SGF), G, gives an exact relation between the internal and scattered fields and the incident fields, $\mathcal{F}^{\mathbf{0}}$, in terms of the surface integral [11].

$$\mathcal{F} = \int_S G\mathcal{F}^{\mathbf{0}} ds, \tag{5}$$

where $\mathcal{F}$ represents the internal fields inside the particle and the scattered fields outside the particle. The SGF is a function solely of the particle in question (not the incident field), and, once calculated, can be used to find the field at any point from any incident field. We show in this section how to find numerically efficient approximations of Eq.(5) by using the boundary conditions.

We can enforce the boundary conditions at the particle surface by matching the expansions of the fields in SVWF's so that the residual of the surface fields is minimised around the particle in a least squares sense. Consider U_α, D_α, an auxiliary system of (possibly generalized) vector functions which are linearly independent and have the component orthogonal to S identically null. Using a finite subset of these functions with $\alpha \leq \alpha_{Max}$, (with $\alpha_{Max} \geq \nu_{Max}$) and the boundary conditions, we can define the matrix equation relating the incident fields , $\mathcal{F}^{\mathbf{0}}$, to the internal and scattered fields

$$\begin{bmatrix} < U_\alpha|F^i_\nu > & < U_\alpha|F^s_\nu > \\ < D_\alpha|F^i_\nu > & < D_\alpha|F^s_\nu > \end{bmatrix} \begin{bmatrix} c^i_\nu \\ -c^s_\nu \end{bmatrix} = \begin{bmatrix} < U_\alpha|\mathcal{F}^{\mathbf{0}} > \\ < D_\alpha|\mathcal{F}^{\mathbf{0}} > \end{bmatrix}, \tag{6}$$

where we use the notation $< a|b >= \int_S a \cdot b ds$ to indicate the surface integral of the scalar product of complex vector functions over the surface S. Note that we can find a least-square solution for the expansion coefficients c^i_ν and c^s_ν even when the left hand side matrix in Eq. 6 is rectangular by calculating, through Singular Value Decomposition (SVD) [13], the Moore-Penrose pseudo-inverse, a generalised matrix inverse defined for non-square complex matrices. By solving Eq. 6, we can find an approximate surface Green function,

$$G^{\nu_{Max},\alpha_{Max}} = [F^i_\nu I_i, -F^s_\nu I_s] L^{-1}_{\nu\alpha} \begin{bmatrix} U_\alpha \\ D_\alpha \end{bmatrix}, \tag{7}$$

where I_i is 1 inside the particle and 0 elsewhere, I_s is 0 inside the particle and 1 elsewhere, and L^{-1} is the pseudo-inverse of the left hand side matrix in Eq.(6). For fixed ν_{Max}, the value of α_{Max} at which one reaches convergence depends on the choice of U_α, D_α. It can be shown that by increasing ν_{Max} and α_{Max}, $G^{\nu_{Max},\alpha_{Max}}$ converges to G [11]. The algorithm requires $O(\alpha^3_{Max})$ operations, but uniquely determines the fields at all points in space. Furthermore, once $G^{\nu_{Max},\alpha_{Max}}$ has been determined, it need not be evaluated for each individual input field, offering a computational saving over methods such as the Finite Difference Time Domain technique.

In this paper we take advantage of the fact that, for axisymmetric scatterers, the azimuthal modes decouple and we can thus project on each harmonic $\exp(im\phi)$ and solve each azimuthal mode individually. We consider particles whose surface can be parametrized by the angles θ and ϕ and use generalised projection functions $|U_\alpha >= [u_\alpha, 0]^T$, $|D_\alpha >= [0, u_\alpha]^T$ with

$$\begin{aligned} u_\alpha \circ \mathcal{S} &\equiv \int \delta(\theta - \theta_p) \frac{e^{-im\phi}}{2\pi} [\hat{n}(\theta) \times \hat{\phi}(\theta,\phi)] \cdot [\hat{n}(\theta) \times \mathcal{S}(\theta,\phi)] d\theta d\phi \\ &= \frac{1}{2\pi} \int e^{-im\phi} [\hat{n}(\theta_p) \times \hat{\phi}(\theta_p,\phi)] \cdot [\hat{n}(\theta_p) \times \mathcal{S}(\theta_p,\phi)] d\phi, \end{aligned} \tag{8}$$

for $1 \leq \alpha \leq \alpha_{Max}$ and

$$u_\alpha \circ \mathcal{S} \equiv \int \delta(\theta - \theta_p) \frac{e^{-im\phi}}{2\pi} \hat{\phi}(\theta, \phi) \cdot [\hat{n}(\theta) \times \mathcal{S}(\theta, \phi)] d\theta d\phi$$
$$= \frac{1}{2\pi} \int e^{-im\phi} [\hat{n}_r(\theta_p) \mathcal{S}_\theta(\theta_p, \phi) - \hat{n}_\theta(\theta_p) \mathcal{S}_r(\theta_p, \phi)] d\phi, \tag{9}$$

for $\alpha_{Max} + 1 \leq \alpha \leq 2\alpha_{Max}$. In this work we choose α as an index for points on the surface where the boundary conditions are matched. $\hat{\phi}$ is the unitary vector along ϕ in spherical polar coordinates, $\delta(\theta_p)$ is the Dirac delta at the point θ_p on the surface of the particle and $\hat{n}(\theta_p) \times \hat{\phi}(\theta_p, \phi), \hat{\phi}(\theta, \phi)$ are tangent to S and orthonormal. This choice of functions leads to the point matching system, where the matrix equations must be overdetermined, i.e. the number of points must be larger than the number of functions used in the expansion of the fields.

2.4. Discrete scattering cross sections and the residual field error

The Differential Scattering Cross Section, DSCS, is the far field angular variation in electric field intensity, and is normally separated into two orthogonal polarisations, the P-polarisation and S-polarisation. It is used in a standard test of the convergence of scattering methods whereby the number of functions used to expand the scattered field is increased to a point where the DSCS remains unchanged. The DSCS of different methods are often compared in literature to ensure various methods produce concurring results. It is given by

$$\sigma^s_{P,S} = \lim_{r \to \infty} |e^{-ik_s r} r \mathbf{E}^{\mathbf{s}}_{\theta,\phi}|^2 \tag{10}$$

We evaluate all scattering cross sections in the $x-z$ plane (the plane shown in Fig. 1).

A much more useful measure of the accuracy of the method for near-field effects is the relative error in the residual at any point, p, on the surface

$$\delta_e = \frac{|\hat{\mathbf{n}}(p) \times (\mathbf{E^0}(p) + \mathbf{E^s}(p) - \mathbf{E^i}(p))|^2}{|\hat{\mathbf{n}}(p) \times \mathbf{E}^0(p)|^2}. \tag{11}$$

It can be shown that this error at the surface of the particle gives the upper bound error at any point in space [14]. Relative fractional errors in the residual of no greater than 10^{-3} are usually deemed acceptable [15], although the magnitude varies with particle composition. This error measure is an excellent method of determining whether the boundary conditions are well matched and, therefore, if the solution is acceptable.

3. Results

By enforcing the boundary condition at the particle surface, we automatically find the field solutions at any point in space and by calculating the residual of the surface fields we find maximal error in the solution. Firstly, in Fig. (2), for spheres, we compare our results with that of Mie theory using widely available routines based on theory presented in [16]. The spheres are illuminated by a plane wave incident along the $+z$ axis (with respect to Fig. 1) that is polarised at 45° to the $x-z$ plane. A polar angle of 0° corresponds to the forward direction, while a polar angle of 180° corresponds to the backward direction. The particle size is characterised by the Size Parameter ($SP = 2\pi a/\lambda$). It can be seen that there is excellent agreement between the results.

In Figs.(3-6) we show several more examples of plots of particles which have been solved using our method, in each case we plot the internal and scattered near field in

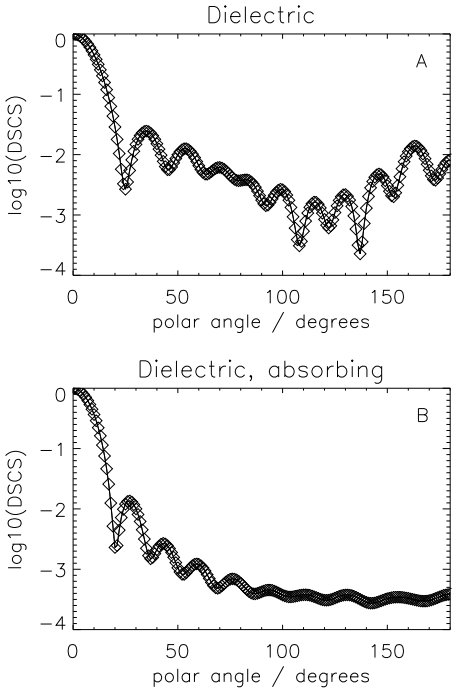

Figure 2. A) Comparison between total DSCS's from our method (data points) and Mie theory (solid line) for a dielectric sphere, refractive index n=1.50, SP=10. Our method was computed for 17 SVWF sources with an average error in the residual of 6.2×10^{-12}. B) Similar comparison for a strongly absorbing dielectric sphere, refractive index n=1.53+0.33i, SP=10. Our method was computed for 22 SVWF sources with an average error in the residual of 9.1×10^{-11}.

terms of electric field intensity plots (on a linear scale), the far field in terms of DSCS's (which we compare, where available, to the results of Doicu *et al.* [17]) and the residual field error on the particle surface. The average relative error is designated by a dotted line. In each case the incident field is the same as in our previous spherical examples. Either the P or the S-polarisation DSCS is shown for each case so that the graphs do not become too difficult to read, although agreement with both P and S-polarisations to known results is excellent for all the cases where a comparison was available. For each particle, as well as the Size Parameter, we specify the Aspect Ratio ($AR = a/b$). For every particle considered below, the maximum relative fractional error in the residual converges below 10^{-3}, which is usually deemed acceptable [15], and in some cases is significantly below this value.

In Fig. 3 we see a dielectric ellipsoid which produces a very localised, intense beam on the shadow side of the particle which is characteristic of a nanojet. In Fig. 4 a dielectric rounded cylinder is shown. Internal structure within the particle can clearly be seen, which is similar in nature to whispering gallery modes observed dielectric spheres [18]. In Fig. 5 we show a dielectric cylinder. Both internal structure and jet like behavior can clearly be seen. Note the ability of the method to handle surfaces with sharp edges, where the boundary conditions Eqs.(2-3) do not formally apply at the edges and the system of SVWF's used to expand the fields is not complete. The

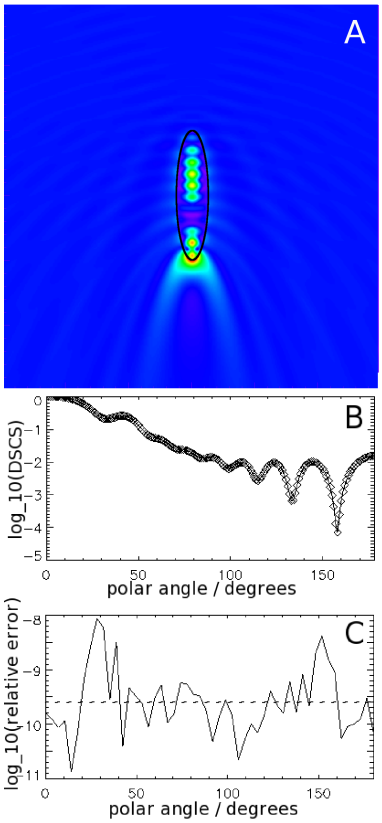

Figure 3. Dielectric ellipsoid, refractive index, n=1.59, SP=13.1, AR=4 computed for 27 SVWF sources. A) Near field intensity plot showing an intense beam on shadow side of particle, with a full width at half maximum of 0.84λ, characteristic of a nanojet. B) DSCS comparison, P-polarisation, solid line results from Doicu *et al.*, data points calculated via our method C) Error in residual; maximum=2.7×10^{-9}, average=2.4×10^{-10}.

method also copes very well with metallic particles, a gold ellipsoid is shown in Fig. 6. No special approximations are made for the boundary of the gold particle; namely, it is not assumed to be a perfect conductor and the internal field is not set to zero. The boundary conditions produce finite fields within the particle which rapidly attenuate as expected since the skin depth is $<< \lambda$. The ability of the method to find internal fields in metallic particles makes it an exciting approach in the study of plasmonics.

4. Summary

We have shown that it is possible to calculate both the near and far field properties, as well as the internal field of dielectric and metallic axisymmetric nanostructures via surface Green functions. By enforcing boundary conditions at the particle surface, we are automatically able to find the field and maximal error at any point in space, including inside the particle. Also, by defining the SGF in terms of distributed lowest order SVWF's, we are able to characterise particles which are elongated from a sphere,

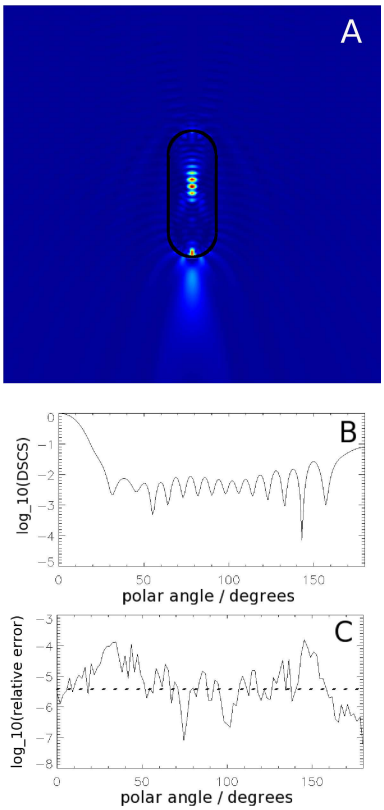

Figure 4. Dielectric rounded cylinder, n=1.59, SP=20.8, AR=2.6 computed for 52 SVWF sources. A) Near field intensity plot. B) DSCS using our method, S-polarisation. Results from literature are not available for comparison. C) Relative error in residual; maximum=1.4×10^{-4}, average=1.8×10^{-5}.

a problem which rapidly produces an ill conditioned set of equations for localised source methods. For each particle, we have shown that the error in the calculation is sufficiently small to ensure accurate results. We have used our method to find DSCS's for the particles which match known results, where results for comparison are available. We have also found, in the near field, internal field structure and nanojets - two interesting phenomena studied widely in literature. The ability of this method to accurately find internal fields in dielectric particles could prove extremely useful in the study of nano-resonators. Furthermore, we are able to find the internal field inside metallic particles, while still enforcing the boundary conditions to a high precision without making approximations about the nature of this field. We believe that this could make this method particularly useful in the field of plasmonics.

References

[1] G. Mie. Beitraege zur Optik trueber Medien, speziell kolloidaler Metalosungen. *Annales de Physik*, 25:337–445, 1908.

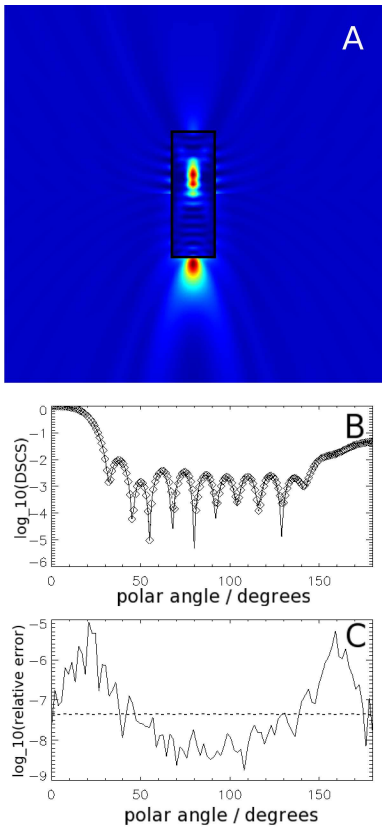

Figure 5. Dielectric cylinder, n=1.59, SP=13.1, AR=4.1 computed for 32 SVWF sources. A) Near field intensity plot showing internal structure and a jet with a full width at half maximum of 0.67λ. B) DSCS comparison, S-polarisation, solid line results from Doicu *et al.*, data points calculated via point matching method. C) Relative error in residual; maximum=9.8×10^{-6}, average=1.2×10^{-7}.

[2] M. El-Sayed. Some Interesting Properties of Metals Confined in Time and Nanometer Space of Different Shapes. *Acc. Chem. Res.*, 34:257–264, 2001.

[3] A. V. Itagi and W. A. Challener. Optics of photonic nanojets. *J. Opt. Soc. Am.*, 22:2847–2858, 2005.

[4] A. Taflove Z. Chen and V. Backman. Photonic nanojet enhancement of backscattering of light by nanoparticles: a potential novel visible-light ultramicroscopy technique. *Optics Express*, 12:1214–1220, 2004.

[5] A.Taflove S. Kong, A.Sahakian and V.Backman. Photonic nanojet-enabled optical data storage. *Optics Express*, 16(18):13713–13719, 2008.

[6] T. Wriedt. E. Eremina, Y. Eremin. Review of light scattering by fiber particles with a high aspect ratio. *Recent Res. Devel. Optics*, 3:297–318, 2003.

[7] S. Dermott E. Green, B.Gustafson. *Interplanetary Dust.* Springer, 2001.

[8] A. Taflove. *Computational electrodynamics: the finite difference time-domain method.* Artech House, 1995.

[9] T. Wriedt A. Doicu. Extended boundary condition method with multipole sources located in the complex plane. *Optics Communications*, 139:85–91, 1997.

[10] M. Kahnert. A. Doicu T. Rother and J. Wauer. Surface Green's functions of the Helmholtz equation in spherical coordinates. *Prog. Electromag. Res.*, 38:47–95, 2002.

[11] T. Rother. Self-consistent Green's function formalism for acoustic and light scattering. *Optics Communications*, 251:254–269, 2005.

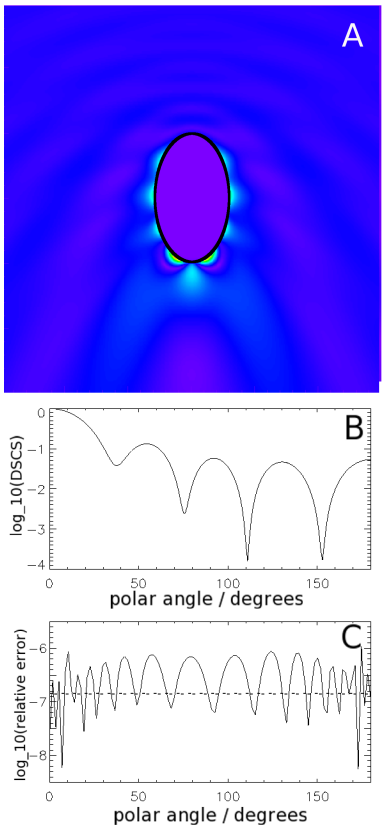

Figure 6. Gold ellipsoid, n=0.33+3.16i, SP=6, AR=2 computed for 21 SVWF sources. A) Near field intensity plot showing rapid decay of field within particle B) DSCS using our method, P-polarisation. Results from literature are not available for comparison. C) Relative error in residual; maximum=1.0×10^{-6}, average=1.1×10^{-7}.

[12] Y. Eremin A. Doicu, T. Wriedt. *Light Scattering by Systems of Particles*, pages 295–301. Springer, 2006.
[13] J. Gentle. *Numerical Linear Algebra for Applications in Statistics*, pages 102–103. Berlin: Springer-Verlag, 1998.
[14] Y. Eremin A. Doicu, T. Wriedt. *Light Scattering by Systems of Particles*, pages 190–191. Springer, 2006.
[15] T. Wriedt E. Eremina, Y. Eremin. *Optics Communications*, 267:524–529, 2006.
[16] D. Bohren and C. Huffman. *Absorption and scattering of light by small particles*, pages 120–123. Wiley, 1983.
[17] Y. Eremin A. Doicu, T. Wriedt. *Light Scattering by Systems of Particles.* Springer, 2006.
[18] A. Taflove Z. Chen. *Opt. Lett.*, 31:389–391, 2006.